Appl Phys B (2009) 97: 181–185
DOI 10.1007/s00340-009-3580-2

Applied Physics B
Lasers and Optics

Grain-size-related transient terahertz mobility of femtosecond-laser-annealed polycrystalline silicon

Y.-C. Wang · H. Ahn · C.-H. Chuang · Y.-P. Ku · C.-L. Pan

Received: 6 January 2009 / Revised version: 28 April 2009 / Published online: 22 May 2009

Abstract We investigated carrier-relaxation dynamics of femtosecond laser annealed (FLA) polycrystalline silicon (poly-Si). The correlation between morphology and electrical properties of poly-Si after femtosecond laser annealing is elucidated by optical-pump–terahertz-probe and terahertz time-domain spectroscopies. The transient conductivities of FLA-processed poly-Si with large (∼500 nm) and small (∼50 nm) grain sizes were both well fitted by the Drude model in the terahertz regime from 0.4 to 2 THz. The transient mobilities of these materials were determined to be 175 ± 19.4 and 94.5 ± 20.2 cm^2/V s, respectively. After annealing, reduction of deep-state density rather than tail-state density in large-grain poly-Si is responsible for its higher mobility.

PACS 78.47.Jc · 72.20.Jv · 68.35.Dv

1 Introduction

Carrier mobility of poly-silicon (poly-Si) is higher than that of amorphous silicon (a-Si). Thus, thin-film transistors (TFTs) fabricated on poly-Si exhibit better electrical characteristics [1–5]. Nevertheless, defects present in poly-Si, such as dangling-bond defects at grain boundaries or strained defects, can reduce the carrier mobility and lead to leakage current, which in turn degrades the performance of TFTs [6, 7]. Typical channel lengths of TFTs are about 5–10 μm. Ideally, this should be close to or smaller than the grain size of poly-Si in order to leave a single grain in the channel area [8, 9]. To obtain poly-Si of large grain sizes, laser or furnace annealing has been successfully employed [5]. Recently, we reported near-infrared femtosecond laser annealing (FLA) for crystallization of a-Si and activation of dopant atoms confined in ultra-shallow junction regions [10, 11]. Characteristics such as field-effect mobility, threshold voltage, and subthreshold slope for FLA-annealed poly-TFTs are found to be comparable to those achieved by conventional approaches [7]. Further, FLA can be achieved at lower laser fluences and exhibits a larger process window than excimer laser annealing (ELA). FLA-processed poly-Si is also superior in terms of surface smoothness.

Since the grain size of poly-Si is one of the key parameters that affects electrical characteristics of TFTs such as mobility, it is important to determine the grain size of poly-Si before TFT fabrication. Traditionally, the grain size is examined by scanning electron microscopy (SEM). However, Secco etching, which is not a nondestructive testing procedure, is required for SEM. On the other hand, THz time-domain spectroscopy (THz-TDS) has been proven as an effective, noncontact method for determination of the electrical characteristics such as conductivity and mobility of semiconductors. Materials relevant to this study, e.g. a-Si, radiation-damaged silicon-on-sapphire (RD-SOS), silicon-on-sapphire (SOS), and nanocrystalline poly-Si, have been investigated by THz-TDS and related spectroscopies [12, 13]. In this paper, we present results on the grain-size-dependent electrical properties of FLA-annealed poly-Si measured by THz-TDS. The temporal evolution of

Y.-C. Wang · H. Ahn · C.-H. Chuang · Y.-P. Ku
Department of Photonics and Institute of Electro-optical Engineering, National Chiao Tung University, Hsinchu 30010, Taiwan

C.-L. Pan (✉)
Department of Physics and Institute of Photonics Technologies, National Tsing Hua University, Hsinchu 30013, Taiwan
e-mail: clpan@phys.nthu.edu.tw
Fax: +886-3-5723052

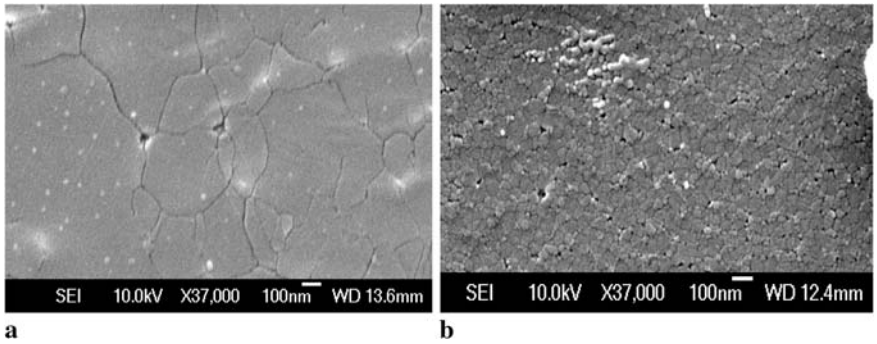

Fig. 1 SEM pictures of poly-Si samples annealed by FLA at (**a**) 45 and (**b**) 34 mJ/cm^2. The average grain sizes of (**a**) and (**b**) are measured to be 500 nm and 50 nm, respectively

the far-infrared conductivity and refractive indices of large- and small-grain poly-Si have also been investigated by the optical-pump–terahertz-probe (OPTP) technique [14]. The quality of poly-Si samples relevant for TFT fabrication was directly identified.

2 Experimental methods

Two poly-Si samples with different grain sizes were prepared by the line-scan FLA technique on 100-nm-thick a-Si layers deposited by low-pressure chemical vapor deposition (LPCVD) at 550°C on SiO_2-coated (500-nm-thick) Si wafers. A 1-kHz Ti:sapphire regenerative amplifier system (RGA), which generates 2-mJ, 50-fs, 800-nm pulses, was employed for both annealing and the optical diagnosis of the samples. Details of the annealing procedure can be found elsewhere [10]. Two poly-Si samples with average grain sizes differing by an order of magnitude were produced from the a-Si layers irradiated with 95% interpulse overlapping at two different laser fluences, 35 and 45 mJ/cm^2, respectively. The morphologies and average size of the poly-Si were analyzed using SEM. For the OPTP experiment, a frequency-doubled (400 nm) photoexciting beam is collimated on the samples with a spot size of ∼3 mm at the angle of incidence of 45°, while the THz probe pulses generated from a photoexcited InAs surface are focused normally on the samples with a spot size of ∼2 mm. The transmitted THz signals were detected by free-space electro-optic sampling in a 2-mm-thick ZnTe crystal as a function of delay time with respect to the optical pulse [15, 16]. The temporal evolution of the refractive indices and the extinction coefficients of the samples were investigated by measuring the transmitted THz signals at a certain pump delay time. The THz spectrometer was purged with dry nitrogen such that a relative humidity, RH $< 7\%$, was maintained throughout the measurements.

3 Results and discussion

The SEM images of poly-Si samples annealed at the pump fluences of 34 and 45 mJ/cm^2 reveal that the average grain sizes are 50 nm (small-grain-size poly-Si, SPSi) for the former and 500 nm (large-grain-size poly-Si, LPSi) for the latter, respectively (see Fig. 1). The performance of TFTs fabricated on similar samples has been discussed in our previous studies [7, 10].

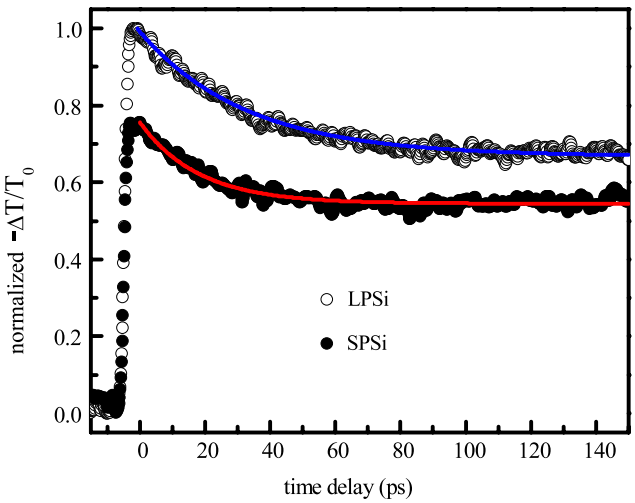

Fig. 2 Differential transmission at the peak of the THz pulse for FLA-processed poly-Si of different grain sizes. LPSi shows stronger absorption of THz radiation than SPSi

Figure 2 shows the normalized differential transmission of SPSi and LPSi excited at the same optical pump fluence of 636 μJ/cm^2. Differential transmission is defined as $-\Delta T/T_0 = -(T - T_0)/T_0$, where T_0 is the peak amplitude of the transmitted THz pulses through the unexcited sample. Although LPSi shows stronger absorption of THz radiation than SPSi, both transmission curves show a subpicosecond onset of the transmission drop followed by a long-term recovery. The decay trend can be fitted by a double-exponential function:

$$\Delta T/T_0 = \Delta T_{\max} \times \left[a\mathrm{e}^{-t/\tau_a} + (1-a)\,\mathrm{e}^{-t/\tau_b}\right], \quad (1)$$

where τ_a and τ_b are the band-to-band carrier recombination time and carrier trapping time, respectively [17]. The best fitting parameters are summarized in Table 1.

Table 1 Fitting parameters of THz differential transmission curves in Fig. 2

	Small grain	Large grain
a	0.713	0.668
τ_a (ns)	92	88
τ_b (ps)	24.4	32.7

As soon as intense blue (400 nm) pump pulses arrive, carriers are generated in the poly-Si samples and they affect the THz probe pulses arriving later. The recovery of THz signals, therefore, is determined by recombination and trapping of the thermalized carriers. Similar transient behavior has been observed for microcrystalline silicon (μc-Si) [17], which exhibits higher defect density and much smaller grain sizes (10–15 nm) compared to our FLA-annealed poly-Si. As a result, μc-Si exhibited fast recovery of THz transients and a trapping time of 0.7 ps. Comparatively longer relaxation times, 24.4 and 32.7 ps, observed for SPSi and LPSi, therefore indicate that both samples have fewer defects to trap the carriers after FLA annealing.

We varied the pump laser fluence from 318 to 955 μJ/cm^2. The measured relaxation time, τ_b, differed at most by ±1.2 ps from a mean value of 32.7 ps over this fluence range. It is well known that the nonlinear Auger recombination process becomes increasingly important with the concentration of injected carriers generated by higher laser fluences [12, 13, 18]. The relatively weak fluence dependence of τ_b, therefore, implies that the Auger recombination process plays a minor role in the carrier-relaxation dynamics for our samples. Consequently, the observed relaxation of the THz transient is mainly due to the trapping of carriers by defect states in poly-Si. Stronger THz absorption observed for LPSi than that for SPSi (see Fig. 2) suggests that, under the same pump fluence, there are more photoexcited carriers left in LPSi, which can strongly absorb the THz signal.

It is well known that the carrier-recombination process in semiconductors is dominant at about ten picoseconds after the optical pump pulse arrives [19]. In order to observe only phenomena induced by carrier trapping, we measured the frequency-dependent dielectric constants of LPSi, SPSi, and a reference (highly resistive Si substrate) by THz-TDS at a fixed time delay of 10 ps. The complex dielectric constant and refractive index are related by $\varepsilon(\omega) = \varepsilon_\infty + i\sigma(\omega)/(\omega\varepsilon_0) = (n + ik)^2$, where ε_0 is the permittivity of free space, $\sigma(\omega)$ is the complex conductivity, and the dielectric constant in the absence of free carriers is $\varepsilon_\infty = 11.7$ [20]. We fitted the measured complex refractive index and conductivity using the simple Drude model, in which the complex conductivity is defined by $\sigma(\omega) = \varepsilon_0\omega_p^2\tau_0/(1 - i\omega\tau_0)$; $\omega_p^2 = Ne^2/(m\varepsilon_0)$ is the plasma frequency, τ_0 the carrier scattering time, and m^* the electron effective mass [21].

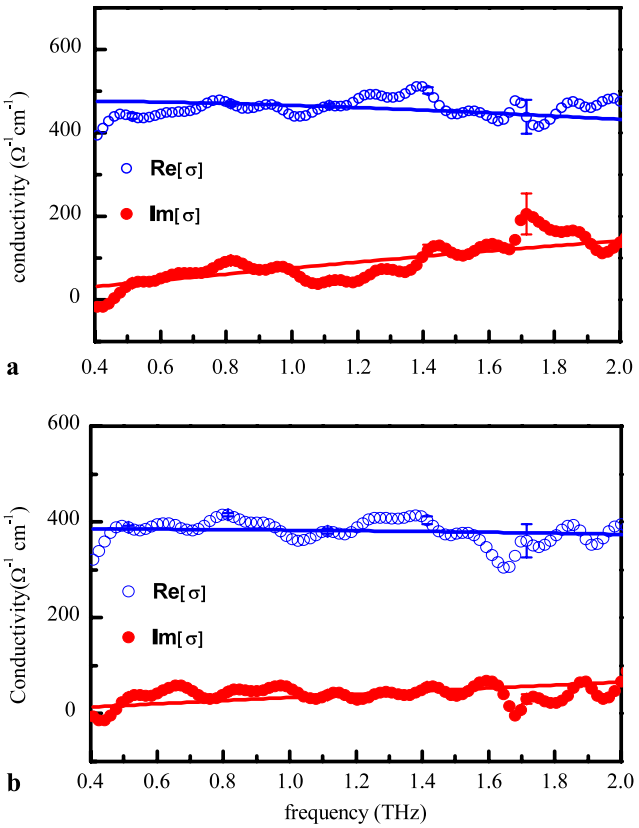

Fig. 3 THz conductivity spectra of (**a**) LPSi and (**b**) SPSi at a fixed time delay of 10 ps. The measured complex refractive indices and conductivities were fitted using the simple Drude model (*solid lines*) to extract plasma frequency and carrier scattering time

Using τ_0 and ω_p extracted from the best fitting of the data and a given value of m^*, the carrier density N and mobility $\mu = e\tau_0/m^*$ can be calculated.

The THz conductivity spectra of LPSi and SPSi at a fixed time delay of 10 ps are shown in Fig. 3a and b, respectively. The real parts of the conductivities of both samples decrease slowly as the frequency increases, while the imaginary parts increase slowly. As shown by the fits in solid lines, the complex conductivities are well described by the simple Drude model. The uncorrelated fluctuation of the observed response may be due to the laser intensity fluctuation and nonuniformity of the annealed samples. Mobilities and plasma frequencies of LPSi, SPSi, and bulk silicon as extracted from the conductivity spectra are summarized in Table 2. The electron mobility of bulk Si was also determined independently by Hall measurement. Because of the high resistivity and low carrier concentration of bulk Si, mobilities with a broad range of values were obtained from the Hall measurement. Nevertheless, these are still consistent with that measured by THz-TDS (see Table 2). The mobility of thin poly-Si with low carrier concentration, on the other hand, cannot be measured by commercial Hall apparatus reliably. For comparison, we also listed the mobilities of a-

Table 2 Fitting parameters of conductivity curves in Fig. 3 by Drude model. For comparison, mobility of bulk Si measured by a Hall apparatus is also shown. The mobilities of bulk Si and poly-Si measured by THz-TDS are the mobilities measured at 10 ps after excitation

Sample	Measurement method	Average grain size (nm)	Mobility ($cm^2/V\,s$)	Plasma frequency (10^{13} Hz)	Carrier scattering time (fs)
Bulk Si	Hall		158–299		
Bulk Si	THz-TDS		263 ± 21.2	7.98 ± 0.21	39 ± 3.1
Poly Si (large grain)	THz-TDS	500	175 ± 19.4	7.26 ± 0.36	26 ± 2.8
Poly Si (small grain)	THz-TDS	50	94.5 ± 20.2	7.20 ± 0.04	14 ± 2.9
a-Si[12]			4.4 ± 0.7		
RD-SOS[12]			(44 ± 11)–(383 ± 94)		
SOS[13]			240 ± 7		
Poly-nc-Si[13]		15–25	30 ± 3		

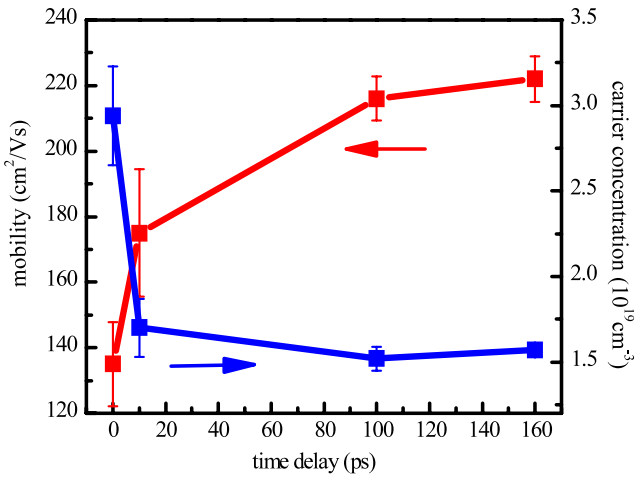

Fig. 4 The mobility and carrier concentration of LPSi are plotted as a function of different optical pump delays. The low mobility at zero optical pump delay induced by carrier–carrier scattering is improved as the carrier concentration becomes lower

Si, radiation-damaged silicon-on-sapphire (RD-SOS) [12], silicon-on-sapphire (SOS) [12], and nanocrystalline poly-Si [13] in Table 2. We note that the mobilities reported in Refs. [12, 13] were also obtained by the fitting of the normalized differential transmission of THz radiation. That is, the conduction mobility is considered to be constant during the carrier trapping or recombination process.

At the optical pumping fluence of 636 μJ/cm^2, we have determined the mobilities and carrier concentrations of LPSi at different optical pump delays. These are plotted in Fig. 4. The fitting result of carrier concentration (2.94×10^{19} cm^{-3}) at zero time delay is in good agreement with the estimated optically injected carrier concentration by the blue pump beam (3.4×10^{19} cm^{-3}). The carrier concentration decreased slightly at longer time delays, while the corresponding mobility rose with the increasing of optical pump delay. The decrease of the carrier concentration may indicate that the available trapping sites are filled up within 10 ps. As a result, only carrier recombination remains at longer time delays. Therefore, the low mobility at zero optical pump delay induced by carrier–carrier scattering will recover as the carrier concentration becomes lower [22]. It is well known that carrier relaxation can depend on the photon energy of the excitation wavelength [16]. This has been seen in the past in GaAs [16]. Previously, Jepsen et al. [17] have reported pump–probe results on microcrystalline silicon with pump wavelengths of 800 and 400 nm. They showed that the time scales of recovery of the normalized transmitted THz signal, $\Delta T/T$, with pump wavelengths at 800 and 400 nm are almost the same. Therefore, the time carriers took after being excited to the satellite valley by 400-nm photons to return to the bottom of the conduction band should be of the order of sub-picoseconds for silicon. In this work, we set the THz probe beam to arrive at the sample 10 ps after the optical pump beam. The mobility measured in this work should not be due to carriers relaxing to the bottom of the conduction band.

The main defects in poly-Si can be categorized into those associated with tail states and deep states. The origins of deep states are dangling bonds at the grain boundaries and interfaces of thin films, while the origins of tail states are intragrain defects [23]. It is well known that both leakage current and mobility of TFTs are more closely associated with trap states located near the band edges due to the band bending at the surface of poly-Si under a positive gate voltage [24, 25]. In this work, however, we measured the conduction mobility instead of the drift mobility, so that the observed transient THz responses are not affected by the tail states. The dangling bonds and tail-state defects have been shown to be responsible for the fast recovery of transmitted THz signals [17, 23, 26]. In our previous study, we showed that poly-Si annealed at higher fluence (~50 mJ/cm^2) and lower

fluence (∼37 mJ/cm^2) exhibit deep-state densities of about 4.3 $\times 10^{17}$ and 1 $\times 10^{18}$ cm^{-3}, respectively [7]. Such a high density of deep states (∼10^{18} cm^{-3}) can significantly reduce the relaxation time of carriers [26]. We also found that poly-Si annealed at higher fluence (∼50 mJ/cm^2) and lower fluence (∼37 mJ/cm^2) exhibit tail-state densities of about 2.7 $\times 10^{20}$ and 5.8 $\times 10^{20}$ cm^{-3}, respectively [7]. However, the tail state may dominate the trapping process only in the sample with a low deep state density (<10^{16} cm^{-3}). Thus, the observed transient THz response in this work should not be affected by the tail states [26]. The penetration depth of poly-Si at 400 nm is between a-Si (14.5 nm) and bulk Si (82 nm); both are shallower than the film thickness of poly-Si. Therefore, the trapping states at a Si/SiO_2 interface can also be neglected. Consequently, we attribute the increase of mobility for LPSi with respect to the SPSi sample to the reduction of dangling bonds in deep states.

4 Conclusion

We used THz spectroscopic techniques to perform non-contact measurements of the electrical characteristics of poly-Si annealed by femtosecond lasers. The complex conductivity of poly-Si was measured in the frequency range from 0.4 to 2 THz. Poly-Si with different grain sizes can be distinguished by optical-pump–terahertz-probe spectroscopy and their transient mobilities are determined non-destructively. From the best fit to the Drude model, the mobilities of the large (∼500 nm)- and small (∼50 nm)-grain-size poly-Si are found to be 175 ± 19.4 cm^2/V s and 95 ± 20.2 cm^2/V s, respectively. The higher mobility of large-grain-size poly-Si is attributed to the reduction of deep-state density rather than that of the tail states, implying the improvement of crystalline quality after FLA.

Acknowledgements This work was supported in part by the National Science Council (NSC) through various grants including PPAEU-II and the Academic Top Universities (ATU) program of the Ministry of Education, Taiwan. The authors would like to thank Mr. H.-M. Li for his assistance in Hall measurements. When the experiments were performed, C.-L. Pan was with the Department of Photonics, National Chiao Tung University. He is now affiliated with the Department of Physics and Institute of Photonics Technologies, National Tsing Hua University, Hsinchu, Taiwan.

References

1. K. Sera, F. Okumura, H. Uchida, S. Itoh, S. Kaneko, K. Hotta, IEEE Trans. Electron Devices **36**, 2868 (1989)
2. E. Ibok, S. Garg, J. Electrochem. Soc. **140**, 2927 (1993)
3. R. Kakkad, J. Smith, W.S. Lau, S.J. Fonash, R. Kerns, J. Appl. Phys. **65**, 2069 (1989)
4. N. Kubo, N. Kusumoto, T. Inushima, S. Yamazaki, IEEE Trans. Electron Devices **40**, 1876 (1994)
5. A.T. Voutsas, Appl. Surf. Sci. **208**, 250 (2003)
6. M. Miyasaka, J. Stoemenos, J. Appl. Phys. **86**, 5556 (1999)
7. Y.C. Wang, J.M. Shieh, H.W. Zan, C.L. Pan, Opt. Express **15**, 6981 (2007)
8. A. Hara, F. Takeuchi, N. Sasaki, in *Proc. 2000 Int. Electron Device Meet* (IEEE Electron Devices Society, New York, 2000), p. 209
9. J.S. Im, R.S. Sposili, M.A. Crowder, Appl. Phys. Lett. **70**, 3434 (1997)
10. J.M. Shieh, Z.H. Chen, B.T. Dai, Y.C. Wang, A. Zaitsev, C.L. Pan, Appl. Phys. Lett. **85**, 1232 (2004)
11. Y.C. Wang, C.L. Pan, J.M. Shieh, B.T. Dai, Appl. Phys. Lett. **88**, 131104 (2006)
12. K.P.H. Lui, F.A. Hegmann, J. Appl. Phys. **93**, 9012 (2003)
13. D.G. Cooke, A.N. MacDonald, A. Hrysiw, J. Wang, Q. Li, A. Meldrum, F.A. Hegmann, Phys. Rev. B **73**, 193311 (2006)
14. M.C. Beard, G.M. Turner, C.A. Schmuttenmaer, J. Phys. Chem. B **106**, 7146 (2002)
15. H. Ahn, C.-H. Chuang, Y.-P. Ku, C.-L. Pan, J. Appl. Phys. **105**, 023707 (2009)
16. M.C. Beard, G.M. Turner, C.A. Schmuttenmaer, Phys. Rev. B **62**, 15764 (2000)
17. P.U. Jepsen, W. Schairer, I.H. Libon, U. Lemmer, N.E. Hecker, M. Birkholz, K. Lips, M. Schall, Appl. Phys. Lett. **79**, 1291 (2001)
18. A. Esser, K. Seibert, H. Kurz, G.N. Parsons, C. Wang, B.N. Davidson, G. Lucovsky, R.J. Nemanich, Phys. Rev. B **41**, 2879 (1990)
19. S.K. Sundaram, E. Mazur, Nature Mater. **1**, 217 (2002)
20. T. Ohba, S. lkawa, J. Appl. Phys. **64**, 4141 (1988)
21. T.-I. Jeon, D. Grischkowsky, Phys. Rev. Lett. **78**, 1106 (1997)
22. D.H. Austo, A.M. Johnson, *Top. Appl. Phys.*, vol. 18 (Springer, Berlin, 1977)
23. N.H. Nickel, G.B. Anderson, R.I. Johnson, Phys. Rev. B **56**, 12065 (1997)
24. T.J. King, M.G. Hack, I.W. Wu, J. Appl. Phys. **75**, 908 (1994)
25. M. Miyasaka, J. Stoemenos, J. Appl. Phys. **86**, 5556 (1999)
26. A.M. Johnson, D.H. Auston, P.R. Smith, J.C. Bean, J.P. Harbison, A.C. Adams, Phys. Rev. B **23**, 6816 (1981)